Applied Physics Letters

Laser cooling of Yb^{3+}:$LuLiF_4$ crystal below cryogenic temperature to 121 K

Cite as: Appl. Phys. Lett. **120**, 231101 (2022); https://doi.org/10.1063/5.0094705
Submitted: 05 April 2022 • Accepted: 23 May 2022 • Published Online: 06 June 2022

Yongqing Lei, Biao Zhong, Tao Yang, et al.

View Online
Export Citation
CrossMark

ARTICLES YOU MAY BE INTERESTED IN

40 GHz waveguide-integrated two-dimensional palladium diselenide photodetectors
Applied Physics Letters **120**, 231102 (2022); https://doi.org/10.1063/5.0091625

Perspective on plexciton based on transition metal dichalcogenides
Applied Physics Letters **120**, 240501 (2022); https://doi.org/10.1063/5.0085435

High-performance broadband photodetector based on $PdSe_2$/black phosphorus heterodiode
Applied Physics Letters **120**, 231103 (2022); https://doi.org/10.1063/5.0097044

QBLOX


1 qubit

Shorten Setup Time
Auto-Calibration
More Qubits

Fully-integrated
Quantum Control Stacks
Ultrastable DC to 18.5 GHz
Synchronized <<1 ns
Ultralow noise


100s qubits

visit our website >

© 2022 Author(s).

Laser cooling of Yb^{3+}:$LuLiF_4$ crystal below cryogenic temperature to 121 K

Cite as: Appl. Phys. Lett. **120**, 231101 (2022); doi: 10.1063/5.0094705
Submitted: 5 April 2022 · Accepted: 23 May 2022 ·
Published Online: 6 June 2022

View Online Export Citation CrossMark

Yongqing Lei,[1] Biao Zhong,[1,a)] Tao Yang,[1,2] Xuelu Duan,[1] Meng Xia,[1] Chaoyu Wang,[1] Jiajin Xu,[1] Ziheng Zhang,[1] Jingxin Ding,[1] and Jianping Yin[1,a)]

AFFILIATIONS

[1]State Key Laboratory of Precision Spectroscopy, East China Normal University, Shanghai 200062, People's Republic of China
[2]Collaborative Innovation Center of Extreme Optics, Shanxi University, Taiyuan, Shanxi 030006, People's Republic of China

[a)]Authors to whom correspondence should be addressed: bzhong@lps.ecnu.edu.cn and jpyin@phy.ecnu.edu.cn

ABSTRACT

Optical cooling techniques of solid-state refrigerators, especially those toward the cryogenic temperature range, have attracted considerable attention in the fields of space exploration, precise measurement, material sciences, and so forth. Here, we report the laser cooling of the 7.5% Yb^{3+}-doped $LuLiF_4$ crystal down to 121 K reaching NIST's designated range of cryogenic temperatures ($<$123 K). Further results based on the cooling window indicate a promising cooling limit of 59 K, provided with enhancement in pump absorbance and heat load management of the sample. Our work, therefore, can motivate an all-solid-state optical refrigeration application beyond the liquid nitrogen boiling point, thus bringing great opportunity to realize cryogenic coolers and radiation-balanced lasers in miniaturized systems.

Published under an exclusive license by AIP Publishing. https://doi.org/10.1063/5.0094705

All-solid-state optical cryo-coolers based on the anti-Stokes fluorescence mechanism can find extensive applications in areas calling for vibration-free and high reliability in cryogenic cooling,[1–6] such as the HgCdTe sensor for infrared detection,[5] silicon single-crystal optical cavities for ultra-stable lasers,[7] and samples for high-resolution electron microscopy.[8] In addition, anti-Stokes fluorescence cooling can help reduce the internal thermal noise and approach the quantum-mechanical ground state of the micro-mechanical systems and nanostructures in combination with the collective photon recoil effect for external cooling.[9–16] Optical tweezers combined with optical cooling can open a new pathway for manipulating microscopic objects in nanotechnology, photonics, and life science.[17–20] Since optical cooling is able to balance the heat generated from quantum defects in solid-state gain media, it will also be beneficial to realize the heat-free-state laser operation and lead to radiation-balanced lasers or athermal lasers.[21–27]

Prior to realization of these promising applications, it is vital to develop laser cooling grade materials that are ideal for optical cryo-coolers practically.[1,15,28–34] In comparison with amorphous glass host materials, crystalline host materials exhibit less inhomogeneous broadening and larger optical absorption coefficients.[35] Fluoride crystals attract the most interest among all kinds of crystalline hosts, largely due to their excellent properties of low phonon energy and low refractive index, leading to low nonradiative relaxation and easy fluorescence escape.[30,36] They also have a characteristic of high transparency in a wide wavelength range spanning from ultra-violet to infrared. Aside from that, fluoride crystals depict a small crystal-field splitting in their ground state that can directly generate a sizeable thermal population in the initial state of the cooling transition at low temperatures, leading to a workable laser cooling efficiency for cryogenic applications.[1,5]

Although net laser cooling was observed in various rare-earth doped materials since Epstein and co-workers' first experimental demonstration,[37] only the 5% Yb^{3+} (co-doped Tm^{3+}):$LiYF_4$ crystal has been optically cooled down to 87 K,[38,39] a temperature point well within the NIST-defined cryogenic temperatures ($<$123 K).[30,40] In terms of a practical application, Hehlen *et al.* developed an optical cryo-cooler using the Yb^{3+}:$LiYF_4$ crystal and cooled an HgCdTe infrared sensor to 135 K[5]. One challenge for growing $LiYF_4$ crystal is that the material melts incongruently, which causes complications during bulky crystal growth in either Czochralski or Bridgman method.[41–44] In contrast, $LuLiF_4$ melts congruently and can form a bulky crystal of better optical quality.[41] Apart from that, $LuLiF_4$ crystals have minor variations with respect to $LiYF_4$ in the coefficients of thermal expansion and thermal conductivity along each crystal axis, leading to more uniform variations in thermal expansion.[45] In addition, the position (58 cm^{-1}) of the lowest peak of phonon density of states in $LuLiF_4$ is lower than that (73 cm^{-1}) in $LiYF_4$.[46] The above-mentioned factors may make the $LuLiF_4$ crystal more suitable for laser cooling than

Published under an exclusive license by AIP Publishing

$LiYF_4$ and motivate researchers to closely investigate their cooling performances of different doping strategies in both crystals.[43,44,47–50] Upon irradiation by a fiber laser of 80 W at 1020 nm, we optically refrigerate a high-purity 7.5% Yb^{3+}-doped $LuLiF_4$ crystal down to 121 K in a double-pass optical geometry, which is the best record ever achieved in this crystal. The contour map of $\eta_c(\lambda, T)$, termed as the cooling window, is also generated based on experimental results, implying that the current crystal can be even potentially cooled down to 59 K, i.e., 18 K below the liquid nitrogen boiling point of 77 K.

Optical cooling of the rare-earth-doped hosts is mainly based on anti-Stokes fluorescence processes.[30,37,51] Rare-earth ions embedded in a transparent host as the coolant are pumped by a laser with the wavelength λ tuned longer than its mean fluorescence wavelength λ_f. Upon the interaction of the crystal field, the $^2F_{7/2}$ and $^2F_{5/2}$ states of Yb^{3+} ions in a $LuLiF_4$ host split into four and three Stark energy levels, respectively. The spontaneously emitted fluorescence photons with higher average energy than the absorbed pump laser photons annihilate the lattice phonons in the host and lead to appreciable cooling. Such an anti-Stokes fluorescence cooling cycle is visualized in Fig. 1(a). The cooling efficiency η_c, which characterizes the laser cooling performance of the sample, can be defined as the ratio of the cooling power P_{cool} to the absorbed power P_{abs},[30,37] i.e.,

$$\eta_c(\lambda, T) = \frac{P_{cool}}{P_{abs}} = \eta_{ext}\frac{\alpha_r(\lambda, T)}{\alpha_r(\lambda, T) + \alpha_b}\frac{\lambda}{\lambda_f(T)} - 1. \quad (1)$$

Here, η_{ext} denotes the external quantum efficiency, which describes the efficiency of fluorescence photons leaving the sample in light of radiative and non-radiative combinations, i.e., $\eta_{ext} = \frac{\eta_e W_r}{\eta_e W_r + W_{nr}}$, where η_e is the fluorescence extraction efficiency and W_r and W_{nr} indicate the radiative and non-radiative recombination rates, respectively. The factor $\alpha_r(\lambda, T)$ represents the resonant absorption coefficient that corresponds to the transition between the top of the ground state and the bottom of the excited state, while α_b represents the background absorption coefficient that originates from all parasitic absorption processes. The mean emission wavelength λ_f (T) can be directly calculated from $\lambda_f(T) = \int \lambda S(\lambda, T) d\lambda / \int S(\lambda, T) d\lambda$,[52] where $S(\lambda, T)$ is the temperature-dependent emission spectrum of the sample. According to the Boltzmann distribution, the resonant absorption coefficient $\alpha_r(\lambda, T)$ can be interpreted as $\alpha_r(\lambda, T) \sim g_v(\lambda, T)\exp[-E_{0i}/k_B T]$, where $g_v(\lambda, T)$ represents the Voigt spectral line.[50] With the decrease in the sample temperature, $\alpha_r(\lambda, T)$ decreases dramatically, and $\lambda_f(T)$ gets red-shifted, thus bringing the cooling efficiency $\eta_c(\lambda, T)$ to cross a zero point. The temperature corresponding to $\eta_c(\lambda, T) = 0$ is called the minimum attainable temperature (MAT) at selected pump laser wavelength λ. The lowest MAT for pump laser wavelength λ varying in the cooling region is called the global MAT (i.e., g-MAT).

It is necessary to enhance the absorption power of the pump laser and minimize the heat load from the environment, prior to obtaining the minimum cooling temperature of the sample. With the sample placed in a high vacuum chamber (10^{-5} Pa), we adopt an optical geometry setup with the pump laser passing through the sample twice in order to enhance the absorption. The heat load power P_{load} on the sample includes the conductive heat load P_{cond}, convective heat load P_{conv}, and the radiative heat load P_{rad}, as indicated in Fig. 1(b). P_{cond} and P_{conv} can be ignored, since the sample is supported by the 100-μm-diameter fiber of low thermal conductivity in the vacuum chamber. When the cooling power P_{cool} balances with P_{rad} on the sample, one can have[30]

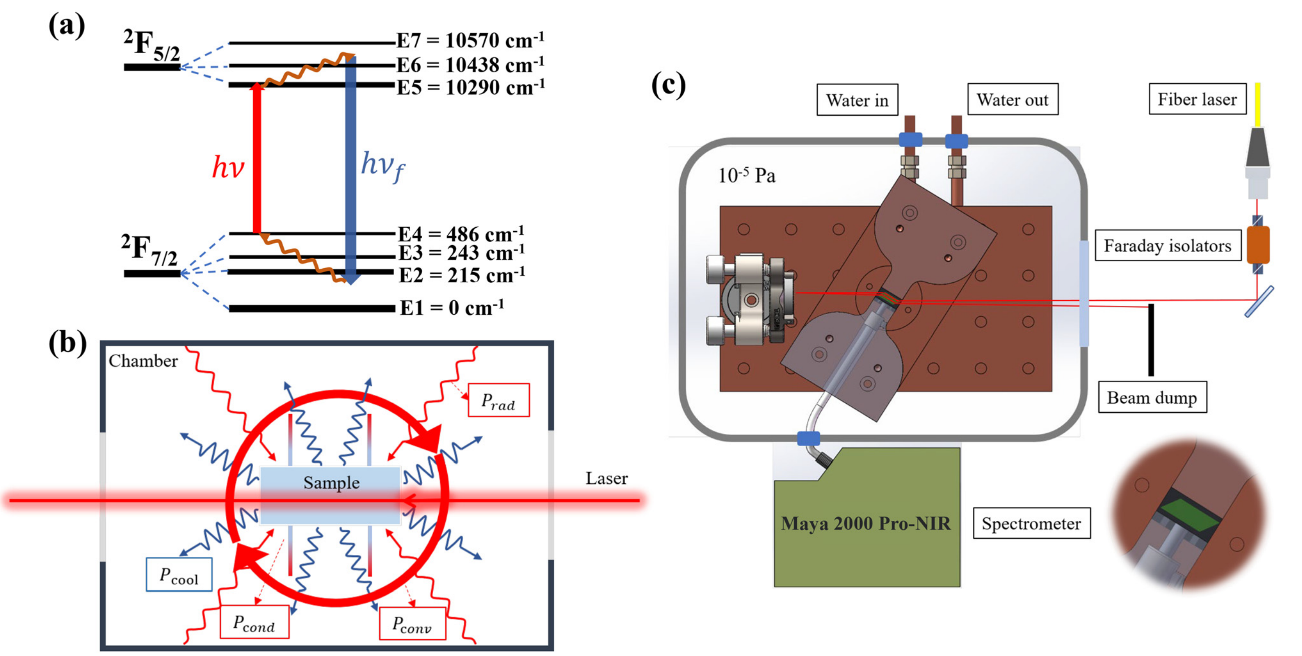

FIG. 1. (a) The Stark sublevel energy diagram for Yb^{3+} ions[53] (not to scale) in $LuLiF_4$ involving absorption (red arrow), anti-Stokes emission (blue arrow), and phonon relaxation (orange arrows). (b) The heat load from three main sources: the convective heat load P_{conv}, the conductive heat load P_{cond}, and the blackbody radiative heat load P_{rad}. (c) Schematic of the experimental setup. A partial enlargement of the clamshell containing the sample is shown in the right corner.

Published under an exclusive license by AIP Publishing

$$\eta_c P_{in}(1 - e^{-2\alpha_r(T)L}) = \frac{\varepsilon_s A_s \sigma}{1+\chi}(T_c^4 - T^4). \quad (2)$$

Here, P_{in}, L, T, and T_c represent the power of the incident pump laser, the length of the sample, the temperature of the sample, and the temperature of the clamshell, respectively. The parameter $\chi = (1-\varepsilon_c)\varepsilon_s A_s/\varepsilon_c A_c$, in which $\varepsilon_{c,s}$ and $A_{c,s}$ represent the emissivity and surface area with the subscripts s and c indicating the sample and its surrounding clamshell, respectively. The Stefan–Boltzmann constant σ is obtained as $5.67\times10^{-8}\,\mathrm{W\,m^{-2}\,K^{-4}}$.

We conducted a few measurements ahead of the laser cooling experiment, including the polarized fluorescence and absorption spectra, the mean fluorescence wavelength, the external quantum efficiency, and the background absorption coefficient. A closed-cycle helium cryostat (Montana) is used to cool the crystal sample, and its temperature can be well regulated by a PID controller in an accuracy of 10 mK within the range of 10–300 K. The polarized fluorescence spectra ($E||$c and $E\perp c$) of the Yb^{3+}:$LuLiF_4$ crystal in the range of 50–300 K are collected by a calibrated fiber spectrometer (Maya 2000 Pro-NIR). Laser-induced thermal modulation spectroscopy (LITMoS) test[39,54] is carried out to evaluate the cooling efficiency $\eta_c^{\exp}(\lambda)$ of the sample pumped at different laser wavelengths, in which $\eta_c^{\exp}(\lambda) = K\Delta T(\lambda)/P_{abs}(\lambda)$. Here, K represents a constant related to the thermal load on the sample, while $P_{abs}(\lambda)$ denotes the absorption pump power that causes the temperature changes ΔT (<5 K) of the sample. The calibrated thermal camera (FLIR A300) and the spectrometer are used to measure ΔT and P_{abs}, respectively. After $\eta_c^{\exp}(\lambda)$ is acquired, the external quantum efficiency η_{ext} and the background absorption coefficient α_b can then be obtained from the model fitting line using Eq. (1).

The schematic of the laser cooling experimental setup is illustrated in Fig. 1(c). A custom-made tunable fiber laser (Precilasers Co., Ltd.) with a maximum output power of 80 W at 1020 nm is used to pump the high-purity 7.5%Yb^{3+}:$LuLiF_4$ crystal. The crystal sample has a size of $2\times2\times10\,\mathrm{mm^3}$ and is supported by two polyimide-coated fibers. The sample is placed in a specially designed copper clamshell, the inner wall of which is coated with a film of high fluorescence absorptivity in the range of 900–1080 nm and low thermal emissivity. The polished crystal with the Brewster-angle cut is laser pumped with respect to the $E||c$ orientation for maximal absorption. The heat load on the crystal is mainly attributed to the blackbody radiation of the environment. A chiller filled with anhydrous ethanol as the coolant is used to remove the heat of the clamshell induced by absorbing the fluorescence from the sample. The fluorescence signal emitted by the crystal is collected by the fiber spectrometer through a hole on the side of the clamshell for temperature monitoring. Differential luminescence thermometry is adopted to determine the temperature of the sample in real time during the laser cooling processes in experiment.[55]

Figure 2(a) shows the fluorescence spectra $S(\lambda, T)$ ($E||c$) of the 7.5%Yb^{3+}:$LuLiF_4$ crystal at different temperatures in the range of 50–300 K at an interval of 50 K. Overall speaking, the fluorescence spectra are getting sharper with the decrease in temperature. The absorption spectra $\alpha_r(\lambda, T)$ for $E||$c are obtained from the fluorescence spectra based on the relation of $\alpha_r(\lambda,T) \propto \lambda^5 S(\lambda,T)e^{hc/\lambda k_B T}$,[52] which can be found in Fig. 2(b). As one can observe, the absorption coefficients drop dramatically with the temperature dropping, particularly in the long wavelength region (>1020 nm). For instance, the absolute value of α_r at 1020 nm decreases in about five orders of magnitude as the temperature changes from 300 to 50 K.

Considering crystal anisotropy, the total mean fluorescence wavelength that different temperatures can be obtained from the expression $\lambda_f(T) = \left(\frac{1}{3}\right)\lambda_f^\pi(T) + \left(\frac{2}{3}\right)\lambda_f^\sigma(T)$.[31] Here $\lambda_f^\pi(T)$ and $\lambda_f^\sigma(T)$ represent the mean fluorescence wavelength of the polarized fluorescence spectra of $E||c$ and $E\perp c$, respectively. The value of $\lambda_f(T)$ can be fitted in a linear temperature dependence as $\lambda_f(T) = (1011.47–0.043\times T)$ nm, which is shown in Fig. 2(c). The LITMoS test results of the sample at room temperature and their theoretical model fitting using Eq. (1) are presented in Fig. 2(d). The cooling efficiency $\eta_c^{\exp}(\lambda)$ is able to be calculated from the measured $P_{abs}(\lambda)$ and ΔT, following which one can derive that $\eta_{ext} = 0.995(\pm0.1)$ and $\alpha_b = 1.4(\pm0.1)\times10^{-4}\,\mathrm{cm^{-1}}$ from Eq. (1). It is clearly to see that net cooling can be achieved when the pump laser wavelength is tuned between 1004 and 1074 nm, as denoted by the blue region.

By measuring cooling parameters, one can determine whether the sample under study is of excellent laser cooling grade. According to the parameters [η_{ext}, α_b, $\alpha_r(\lambda,T)$, and $\lambda_f(T)$] obtained above, the cooling efficiency $\eta_c(\lambda,T)$ of the 7.5% Yb^{3+}:$LuLiF_4$ crystal as a function of the pump laser wavelength λ and the temperature T, so-called cooling window, is plotted in Fig. 2(e). The black dotted line in Fig. 2(e) represents the boundary with $\eta_c(\lambda,T) = 0$, along which the MAT is reached for the corresponding pump laser wavelength. It is noted that the g-MAT of the sample can be as low as ∼103 K when being pumped at 1020 nm, corresponding to the E4 → E5 transition between the $^2F_{7/2}$ and $^2F_{5/2}$ manifolds of Yb^{3+} doped in $LuLiF_4$ crystal. Recent experimental results of elaborate low-temperature LITMoS tests in the Yb^{3+}:$LiYF_4$ crystal reveal that the background absorption coefficient α_b induced by the transition metal ion impurity does not remain constant but decreases in the form of a Boltzmann-type function when the sample temperature changes.[39] Assume the performance of α_b in the Yb^{3+}:$LuLiF_4$ crystal can be expressed by a similar function of temperature as $\alpha_b(T) = 5.1\times e^{-387.6/T}\,10^{-4}\,\mathrm{cm^{-1}}$, a revised contour map of $\eta_c(\lambda,T)$ can be generated, as shown in Fig. 2(f). The final g-MAT is found to be as low as 59 K.

The temperature evolution of the 7.5%Yb^{3+}:$LuLiF_4$ crystal irradiated by the 80 W pumping laser at 1020 nm is shown in Fig. 3(a). After about 20 min of irradiation, the sample is laser-cooled to a final steady-state of a temperature of 121.0 K. According to the expression that $P_{abs} = P_{in}\,[1-\exp(-2a_r L)]$, the absorbed pump power is estimated to be about 7.3 W. The temperature of the clamshell is increased from 253.8 to 265.6 K due to absorption of the fluorescence emitted by the sample. The temperature difference between the crystal sample and the clamshell is about 145.0 K after reaching the steady-state equilibrium. The heat load from blackbody radiation of the clamshell is estimated to be about 11.5 mW.

The dependence of the steady-state temperature of 7.5%Yb^{3+}:$LuLiF_4$ crystal on the pump power of the 1020 nm laser is also investigated, as shown with black solid dots in Fig. 3(b). The final temperature of the sample decreases with increasing pump power. The optical pump rate on the absorption transition is greater than the radiation relaxation rate, resulting in a significant decrease in the number of electron dwellings at the absorption level.[56] It is necessary to consider the effect of saturation absorption particularly at low temperatures.[2,57] The revised resonance absorption coefficient α_r' is closely related to the saturation intensity and can be described as

Published under an exclusive license by AIP Publishing

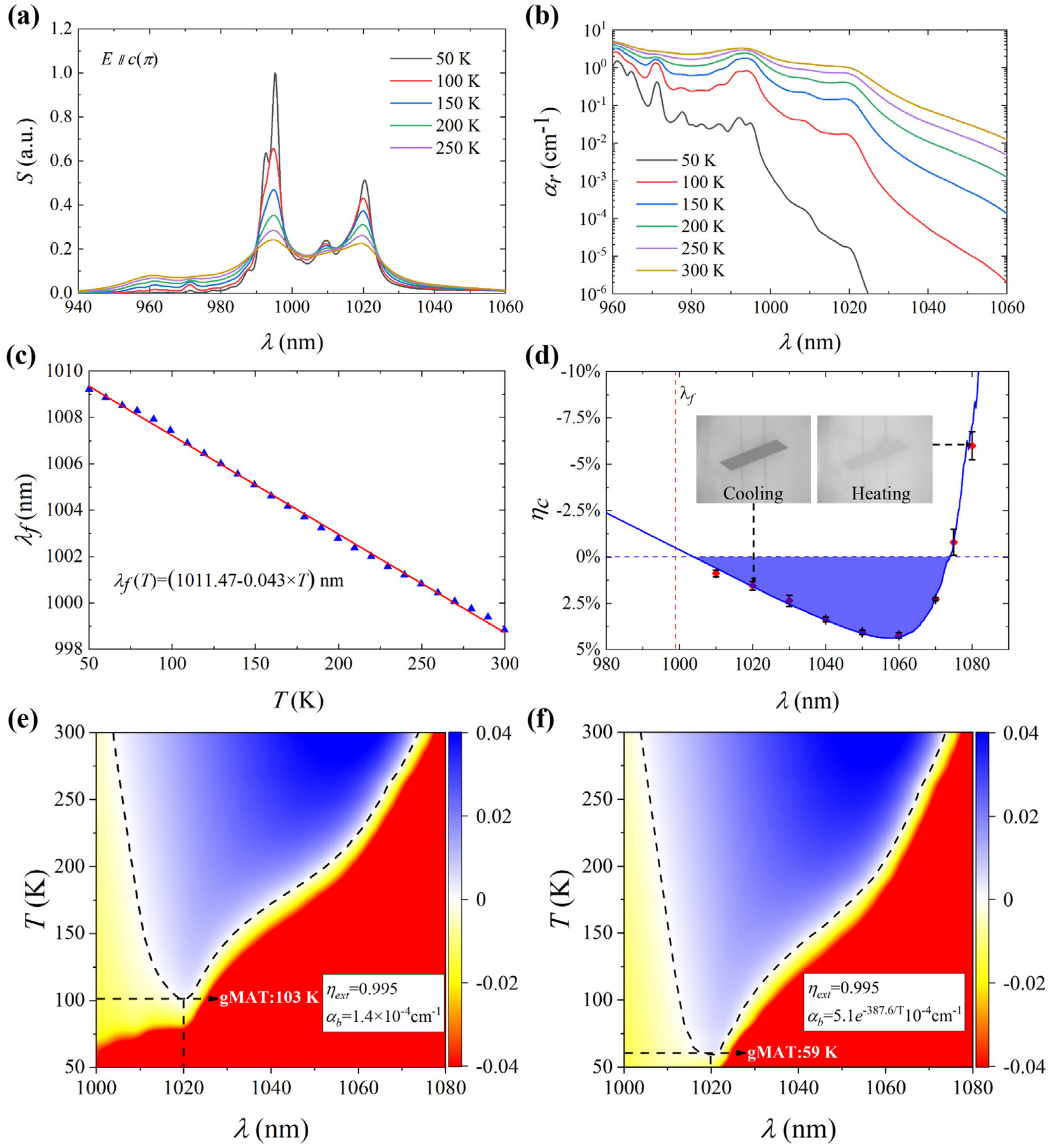

FIG. 2. (a) Temperature-dependent fluorescence spectra of Yb^{3+}:$LuLiF_4$ crystal ($E||c$). (b) The absorption spectrum $\alpha_r(\lambda, T)$ obtained from the fluorescence spectrum ($E||c$) according to the reciprocity relationship. (c) Dependence of the mean fluorescence wavelength on the sample temperature. (d) The LITMoS test results and the fitting curve using Eq. (1). The insets show the thermal images of the sample at 1020 and 1080 nm excitation, respectively. (e) Cooling efficiency contour map η_c (λ, T) for the 7.5% Yb^{3+}:$LuLiF_4$ crystal. Blue region denotes cooling, and red region denotes heating. (f) Cooling efficiency contour map η_c (λ, T) for the 7.5% Yb^{3+}:$LuLiF_4$ crystal in light of the background absorption as a function of the sample temperature.

$\alpha_r'(I) = \alpha_r/(1 + I/I_s)^C$,[58,59] where α_r is the unsaturated resonant absorption coefficient, I and I_s are the pump laser intensity and the saturation intensity, respectively, and C is a crystal-dependent constant and taken as unity here. With the increase in the pump laser power, the value of α_r' is reduced, so is the absorption efficiency η_{abs} and the cooling efficiency η_c. This effect can be understood mathematically as an increase in the effective background absorption α_b', which is given as $\alpha_b' = \alpha_b(1 + I/I_s)$. Here, we adopt that $I_s = 11.45\,\mathrm{kW/cm^2}$ for simplicity to avoid dependences of cooling characteristic on the pump intensity at various temperatures.[56,60] Taking into account of the saturation absorption effect, the absorption efficiency term in Eq. (1) can be revised as $\eta_{abs} = [1 + \alpha_b'/\alpha_r]^{-1}$.[2] Utilizing the above-mentioned cooling parameters and Eq. (2), the mathematical relationship between the steady-state temperature and the pump laser power could be attained, which tends to increase after decrease as denoted by the blue line in Fig. 3(b). The pump power at the turning point is estimated to be 136 W, and the increase in the steady-state temperature for pump power larger than 136 W is mostly ascribed to the saturation

Published under an exclusive license by AIP Publishing

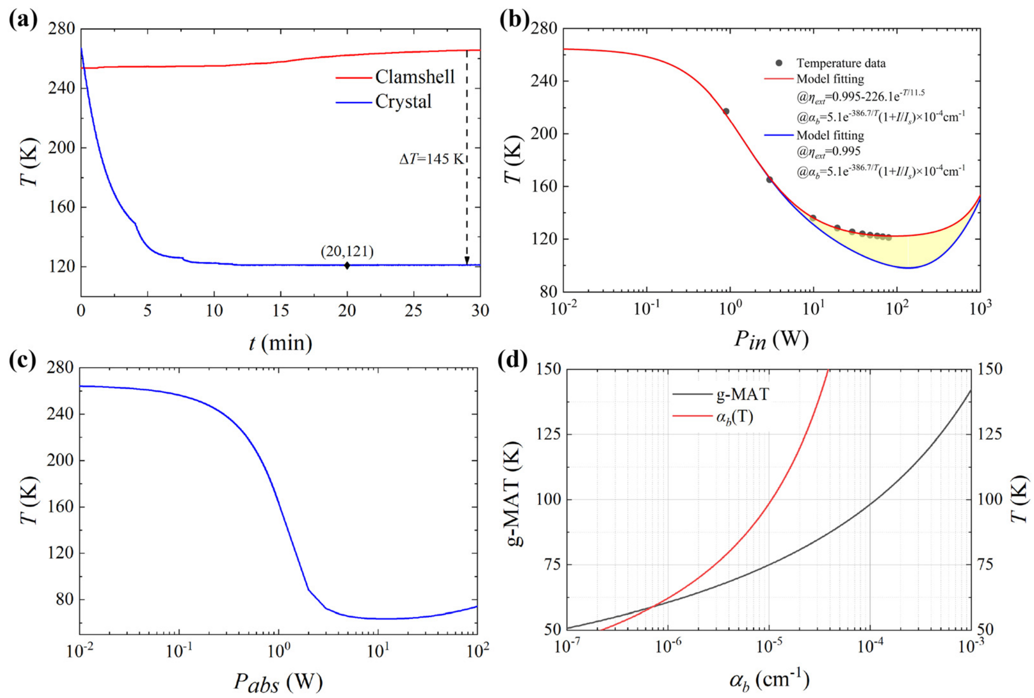

FIG. 3. (a) Time-dependent temperature evolution of the crystal. (b) The measured steady-state temperature of the crystal under different pump laser power and model fitting using Eq. (2) with $I_s = 11.45\,\mathrm{kW/cm^2}$. The yellow region indicate that the water condensation effect plays an important role on the final steady-state temperature of the sample. (c) The cooling temperature from model fitting using Eq. (2) vs absorbed pump laser power considering the saturation absorption effect. (d) Dependence of the effective background absorption on the sample temperature and the g-MAT of the sample predicted from the theoretical model.

absorption effect. Discrepancy emerges between the blue fitting line and the experimental data when the incident laser power exceeds about 10 W, corresponding to a steady-state temperature of 140 K. Such a discrepancy is mainly due to the icy film formation of water molecules upon the sample surface, leading to the descending fluorescence escape rates on the sample as well as the external quantum efficiency η_{ext}. The water saturation vapor pressure is about $\sim 10^{-5}$ Pa at temperatures about 150 K. According to the analysis of the Arden–Buck equation[61] and the experimental data in Fig. 3(b), we obtain $\eta_{ext} = 0.995–226.1e^{-T/11.5}$ during the data fitting process, which is used to characterize the effect of water condensation on the cooling performance of the sample.

It is noteworthy to mention that the cooling performance depends on how much pump laser power is actually absorbed by the sample. Utilizing the cooling parameters obtained in the experiment and considering the above-mentioned saturation absorption effect, we also unveil the relationship between the steady-state temperature and the absorbed power of the pump laser, as shown in Fig. 3(c). If the absorption power can be increased up to about 10 W, the sample under our study can be laser-cooled to the lowest temperature of 63.5 K. The absorption efficiency for our current double-pass pump laser geometry is only about 9%, which can be greatly improved utilizing the non-resonant cavity enhancement absorption. For instance, an Astigmatic Herriott cell can increase the absorption efficiency of the pump laser power up to 90% by letting the laser pass through the sample hundreds of times[62] and avoid the saturation effect caused by excessive laser power.

According to the recent study,[39] the background absorption coefficient $\alpha_b(T)$ decreases with the sample temperature in the form of a Boltzmann-type function, $\alpha_b(T) = 5.1 \times \mathrm{e}^{-387.6/\mathrm{T}}\, 10^{-4}\,\mathrm{cm}^{-1}$, as shown by the red line in Fig. 3(d), in contrast to the dependence of the g-MAT for the 7.5% Yb^{3+}:$LuLiF_4$ crystal on $\alpha_b(T)$ given by the black line. When the sample is being cooled, both $\alpha_b(T)$ and the corresponding g-MAT decrease, which cross at the temperature point of 59 K. When the sample temperature reaches the g-MAT, net cooling ceases and the steady-state is obtained.

Compared with previous works,[47] the quality and the purity of the sample here are much improved. In addition, the reduced heat load as well as the enhanced pump power dramatically improve the laser cooling performances of the 7.5%Yb^{3+}:$LuiLiF_4$ crystal. Note that the 5% Yb^{3+}/Tm^{3+}:$LiYF_4$ crystal holds the current record of the lowest cooling temperature for solid-state laser cooling as 87 K.[38] The achievement of this record is mainly attributed to more efficient thermal load management and enhanced absorption. However, the predicted g-MAT about of 59 K for our sample is lower than that of about 70 K for 5% Yb^{3+}/Tm^{3+}:$LiYF_4$, largely due to the high purity and the high Yb^{3+} doping concentrations. Therefore, based on technical improvements, our sample has relatively great potential for laser cooling. Improving the absorption power of the pumping laser by utilizing the astigmatic Herriott cavity and eliminating the condensation effect of the water in the vacuum chamber will be carried out in our following experimental work in order to justify the better laser cooling performance of the 7.5%Yb^{3+}:$LuLiF_4$ crystal toward the temperature limit of 59 K.

Published under an exclusive license by AIP Publishing

As a conclusion, we have laser-cooled the 7.5% Yb^{3+}-doped $LuLiF_4$ crystal down to 121 K reaching NIST's designated range of cryogenic temperatures (<123 K). In the experimental setup of a double-pass optical geometry, the absorption efficiency of the pump power from the 1020 nm fiber laser is estimated to be about 9%. We present that the saturation absorption effect under strong pump laser power is a major factor affecting the final g-MAT of the sample. Aside from that, the condensation of water vapor upon the sample surface is severely adverse to the laser cooling performance, particularly at low temperatures. The characterization of the cooling windows implies that with further improvement in the pump laser absorbance and heat load management, the sample can be potentially cooled below the liquid nitrogen boiling point of 77 K and eventually reached the temperature as low as 59 K. In the Bridgman crystal growth method, Yb^{3+}-doped $LuLiF_4$ crystals may have better quality than their $LiYF_4$ counterparts, thus they can serve as an excellent candidate for all-solid-state laser coolers and radiation-balanced lasers.

We thank Professor M. Tonelli and Dr. J. W. Meng for helpful discussions and Professor W. Xie for helpful discussions and provision of a closed-cycle helium cryostat. Biao Zhong thanks L. Z. Deng for helpful discussions. This research was partially supported by the National Natural Science Foundation of China (Nos. 11604100, 11834003, and 11874151), the Special Financial Grant from the China Postdoctoral Science Foundation (No. 2016T90346), the Young Top-Notch Talent Support Program of Shanghai, the Program for Professor of Special Appointment (Eastern Scholar) at Shanghai Institutions of Higher Learning, and 111 Project (No. B12024).

AUTHOR DECLARATIONS

Conflict of Interest

The authors have no conflicts to disclose.

Author Contributions

Yongqing Lei: Data curation (equal); formal analysis (equal); investigation (equal); writing – original draft (equal); writing – review and editing (equal). **Biao Zhong:** Conceptualization (lead); data curation (equal); formal analysis (equal); investigation (equal); project administration (lead); writing – original draft (equal); writing – review and editing (lead). **Tao Yang:** Writing – review and editing (supporting). **Xuelu Duan:** Software (supporting). **Meng Xia:** Software (supporting). **Chaoyu Wang:** Investigation (supporting). **Jiajin Xu:** Data curation (supporting). **Ziheng Zhang:** Formal analysis (supporting). **Jingxin Ding:** Writing – review and editing (supporting). **Jianping Yin:** Conceptualization (supporting); project administration (supporting); writing – review and editing (supporting).

DATA AVAILABILITY

The data that support the findings of this study are available from the corresponding authors upon reasonable request.

REFERENCES

[1] D. V. Seletskiy, R. Epstein, and M. Sheik-Bahae, Rep. Prog. Phys. **79**(9), 096401 (2016).
[2] D. V. Seletskiy, M. P. Hehlen, R. I. Epstein, and M. Sheik-Bahae, Adv. Opt. Photonics **4**(1), 78 (2012).
[3] M. Sheik-Bahae and R. I. Epstein, Nat. Photonics **1**(12), 693 (2007).
[4] O. Graydon, Nat. Photonics **12**(6), 315 (2018).
[5] M. P. Hehlen, J. Meng, A. R. Albrecht, E. R. Lee, A. Gragossian, S. P. Love, C. E. Hamilton, R. I. Epstein, and M. Sheik-Bahae, Light. Sci. Appl. **7**(1), 15 (2018).
[6] G. Nemova, *Laser Cooling: Fundamental Properties and Applications* (Jenny Stanford Publishing, 2016).
[7] T. Kessler, C. Hagemann, C. Grebing, T. Legero, U. Sterr, F. Riehle, M. J. Martin, L. Chen, and J. Ye, Nat. Photonics **6**(10), 687 (2012).
[8] E. Callaway, Nature **550**(7675), 167 (2017).
[9] A. T. M. A. Rahman and P. F. Barker, Nat. Photonics **11**(10), 634 (2017).
[10] S. S. Rudyi, T. A. Vovk, A. V. Kovalev, V. M. Polyakov, A. V. Ivanov, E. Y. Perlin, and Y. V. Rozhdestvensky, J. Opt. Soc. Am. B **34**(12), 2441 (2017).
[11] A. Pant, X. Xia, E. J. Davis, and P. J. Pauzauskie, Nat. Commun. **11**(1), 3235 (2020).
[12] J. Chan, T. Alegre, A. H. Safavi-Naeini, J. T. Hill, A. Krause, S. Gröblacher, M. Aspelmeyer, and O. Painter, Nature **478**(7367), 89 (2011).
[13] Y. Seis, T. Capelle, E. Langman, S. Saarinen, E. Planz, and A. Schliesser, arXiv:2107.05552 (2021).
[14] S. Zhang, M. Zhukovskyi, B. Jankó, and M. Kuno, NPG Asia Mater. **11**(1), 54 (2019).
[15] J. Zhang, D. Li, R. Chen, and Q. Xiong, Nature **493**(7433), 504 (2013).
[16] J. Zhang, Q. Zhang, X. Wang, L. C. Kwek, and Q. Xiong, Nat. Photonics **10**, 600 (2016).
[17] J. Li, Z. Chen, Y. Liu, P. S. Kollipara, Y. Feng, Z. Zhang, and Y. Zheng, Sci. Adv. **7**(26), eabh1101 (2021).
[18] P. Y. Chiou, A. T. Ohta, and M. C. Wu, Nature **436**(7049), 370 (2005).
[19] L. Lin, M. Wang, X. Peng, E. N. Lissek, Z. Mao, L. Scarabelli, E. Adkins, S. Coskun, H. E. Unalan, B. A. Korgel, L. M. Liz-Marzan, E. L. Florin, and Y. Zheng, Nat. Photonics **12**(4), 195 (2018).
[20] C. Hong, S. Yang, and J. C. Ndukaife, Nat. Nanotechnol. **15**(11), 908 (2020).
[21] S. R. Bowman, IEEE J. Quantum Electron. **35**(1), 115 (1999).
[22] M. Peysokhan, E. Mobini, A. Allahverdi, B. Abaie, and A. Mafi, Photonics Res. **8**(2), 202 (2020).
[23] M. Sheik-Bahae and Z. Yang, IEEE J. Quantum Electron. **56**(1), 1–19 (2020).
[24] J. M. Knall and M. J. Digonnet, J. Lightwave Technol. **39**(8), 2497 (2021).
[25] J. M. Knall, M. Engholm, T. Boilard, M. Bernier, and M. J. F. Digonnet, Phys. Rev. Lett. **127**(1), 013903 (2021).
[26] J. Knall, M. Engholm, T. Boilard, M. Bernier, P. B. Vigneron, N. Yu, P. D. Dragic, J. Ballato, and M. J. F. Digonnet, Optica **8**(6), 830 (2021).
[27] Z. Yang, J. Meng, A. R. Albrecht, and M. Sheik-Bahae, Opt. Express **27**(2), 1392 (2019).
[28] C. W. Hoyt, M. Sheik-Bahae, R. I. Epstein, B. C. Edwards, and J. E. Anderson, Phys. Rev. Lett. **85**(17), 3600 (2000).
[29] J. Fernandez, A. J. Garcia-Adeva, and R. Balda, Phys. Rev. Lett. **97**(3), 033001 (2006).
[30] D. V. Seletskiy, S. D. Melgaard, S. Bigotta, A. D. Lieto, M. Tonelli, and M. Sheik-Bahae, Nat. Photonics **4**(3), 161 (2010).
[31] S. Rostami, A. R. Albrecht, A. Volpi, and M. Sheik-Bahae, Photonics Res. **7**(4), 445 (2019).
[32] M. Sheik-Bahae and R. I. Epstein, Phys. Rev. Lett. **92**(24), 247403 (2004).
[33] S.-T. Ha, C. Shen, J. Zhang, and Q. Xiong, Nat. Photonics **10**(2), 115 (2016).
[34] B. Zhong, Y. Lei, X. Duan, T. Yang, and J. Yin, Appl. Phys. Lett. **118**(13), 131104 (2021).
[35] X. Xia, A. Pant, A. S. Ganas, F. Jelezko, and P. J. Pauzauskie, Adv. Mater. **33**(23), 1905406 (2021).
[36] M. P. Hehlen, M. Sheik-Bahae, R. I. Epstein, S. D. Melgaard, and D. V. Seletskiy, J. Mater. Chem. C **1**(45), 7471 (2013).
[37] R. I. Epstein, M. I. Buchwald, B. C. Edwards, T. R. Gosnell, and C. E. Mungan, Nature **377**(6549), 500 (1995).
[38] A. Gragossian, M. Ghasemkhani, J. Meng, A. Albrecht, M. Tonelli, and M. Sheik-Bahae, Proc. SPIE **2017**, 2–4.
[39] A. Volpi, J. Meng, A. Gragossian, A. R. Albrecht, S. Rostami, A. D. Lieto, R. I. Epstein, M. Tonelli, M. P. Hehlen, and M. Sheik-Bahae, Opt. Express **27**(21), 29710 (2019).
[40] S. D. Melgaard, D. V. Seletskiy, A. D. Lieto, M. Tonelli, and M. Sheik-Bahae, Opt. Lett. **38**(9), 1588 (2013).

Published under an exclusive license by AIP Publishing

[41]A. Volpi, J. Kock, A. R. Albrecht, M. Sheik-Bahae, and M. P. Hehlen, Proc. SPIE **2021**, 11702.
[42]A. Volpi, J. Meng, A. R. Albrecht, M. Sheik-Bahae, D. Biner, K. W. Krämer, and M. P. Hehlen, Proc. SPIE **10936**, 109360P (2019).
[43]A. Volpi, K. W. Krämer, D. Biner, B. Wiggins, J. Kock, A. R. Albrecht, E. J. Peterson, M. N. Spilde, M. Sheik-Bahae, and M. P. Hehlen, Cryst. Growth Des. **21**(4), 2142 (2021).
[44]E. A. Dobretsova, X. Xia, A. Pant, M. B. Lim, M. C. De Siena, K. N. Boldyrev, A. D. Molchanova, N. N. Novikova, S. A. Klimin, and M. N. Popova, Laser Photonics Rev. **15**(10), 2100019 (2021).
[45]A. Volpi, "Laser cooling of fluoride crystals," Ph. D. (Universita di Pisa, 2015).
[46]A. Sen, S. Chaplot, and R. Mittal, Phys. Rev. B **64**(2), 024304 (2001).
[47]B. Zhong, J. Yin, Y. Jia, L. Chen, Y. Hang, and J. Yin, Opt. Lett. **39**(9), 2747 (2014).
[48]A. Volpi, G. Cittadino, A. D. Lieto, A. Cassanho, H. P. Jenssen, and M. Tonelli, Opt. Eng. **56**(1), 011105 (2016).
[49]B. Zhong, Y. Lei, H. Luo, Y. Shi, T. Yang, and J. Yin, J. Lumin. **226**, 117472 (2020).
[50]G. Lei, J. Anderson, M. Buchwald, B. Edwards, and R. Epstein, Phys. Rev. B **57**(13), 7673 (1998).
[51]P. Pringsheim, Z Phys. **57**(11), 739 (1929).
[52]S. D. Melgaard, *Cryogenic Optical Refrigeration: Laser Cooling of Solids Below 123 K* (The University of New Mexico, 2013).
[53]W. Feng, T. Zeng, M. Zhao, and X. Li, Optik **123**(8), 720 (2012).
[54]X. Duan, B. Zhong, Y. Lei, C. Wang, J. Xu, Z. Zhang, J. Ding, and J. Yin, Appl. Sci. **12**(9), 4447 (2022).
[55]B. Imangholi, M. P. Hasselbeck, D. A. Bender, C. Wang, M. Sheik-Bahae, R. I. Epstein, and S. Kurtz, in *Paper presented at the Physics and Simulation of Optoelectronic Devices XIV* (2006).
[56]Y. Sato and T. Taira, IEEE J. Quantum Electron. **40**(3), 270 (2004).
[57]A. Ivanov, Y. Rozhdestvensky, and E. Perlin, Appl. Opt. **55**(28), 7764 (2016).
[58]A. E. Siegman, *Lasers* (University Science Books, 1986).
[59]T. V. Joseph, *Laser Electronics* (Prentice Hall, Englewood Cliffs, NJ, 1995).
[60]A. Volpi, J. Kock, A. R. Albrecht, M. P. Hehlen, R. I. Epstein, and M. Sheik-Bahae, Opt. Lett. **46**(6), 1421 (2021).
[61]V. Nesterov, M. Gricenko, and T. Shabulina, Hydrol. Meteorol. **9**, 102 (1968).
[62]A. Gragossian, J. Meng, M. Ghasemkhani, A. R. Albrecht, and M. Sheik-Bahae, Opt. Eng. **56**(1), 011110 (2016).

Published under an exclusive license by AIP Publishing